Atomic model of anti-phase boundaries in a face-centred icosahedral Zn–Mg–Dy quasicrystal

Atomic model of anti-phase boundaries in a face-centred icosahedral Zn–Mg–Dy quasicrystal

Jianbo Wang[1,2]**, Wenge Yang**[3] **and Renhui Wang**[1,2]

[1] Department of Physics, Wuhan University, Wuhan 430072, People's Republic of China
[2] Centre for Electron Microscopy, Wuhan University, Wuhan 430072, People's Republic of China
[3] Solid State Division, Oak Ridge National Laboratory, PO Box 2008, Oak Ridge,
TN 37831, USA

E-mail: wang@whu.edu.cn (Jianbo Wang)

Abstract
An atomic model in the physical space for an anti-phase boundary (APB) in the
ordered face-centred icosahedral Zn–Mg–Dy quasicrystal phase is presented,
based on a six-dimensional model suggested by Ishimasa and Shimizu (2000
Mater. Sci. Eng. A **294–296** 232, Ishimasa 2001 private communication). The
physical space atomic positions of the defected structure were used for the
calculation of the corresponding exit-plane wavefunction and high-resolution
transmission electron microscopy images. The analysis of the defect by inverse
Fourier transformation reveals that when superstructure reflection spots are used
for back-transformation, then at the APB, bright lattice fringes are found to
turn into dark ones, and vice versa. When fundamental reflections are used,
the APB is not visible. This phenomenon is the same as the corresponding
experimental study recently published by Heggen *et al* (2001a *Phys. Rev.* B **64**
014202). Based on this atomic model it is found that the APB perpendicular
to a fivefold axis A5 (APB-A5) is a non-conservative boundary, while the APB
perpendicular to a pseudo-twofold axis A2P (APB-A2P) is a conservative one.
This fact is consistent with the experimental observation (Heggen *et al* 2002
J. Alloys Compounds **342** 330) that the frequency of occurrence of APB-A5 is
90% in the heat-treated samples compared with that in the deformed samples
(45%), while the frequency of occurrence of APB-A2P is 34% in the deformed
samples compared with that in the heat-treated samples.

1. Introduction

Since the first observation of an icosahedral quasicrystal (IQC) in a Zn–Mg–RE (RE = rare-
earth element) alloy system by Luo *et al* (1993), and a highly ordered face-centred IQC phase
was reported by Niikura *et al* (1994a, 1994b) and Tsai *et al* (1994), this new class of IQCs

triggered brisk experimental activity mainly for the following two reasons. Firstly, comparing with the intensively studied Al-based IQCs (e.g., Al–Pd–Mn and Al–Cu–Fe), these novel highly perfect and thermodynamically stable IQCs have different atomic structures (Yamamoto *et al* 1996, Ohno and Ishimasa 1998, Ishimasa and Shimizu 2000, Takakura *et al* 2001) and physical properties (Fisher *et al* 1998). Secondly, these IQCs provide the opportunity to investigate magnetism involving localized 4f moments on RE sites in a quasi-periodic lattice (Charrier *et al* 1997, Sato *et al* 1998b, Matsuo *et al* 2000). This in turn inspired the search for quasicrystals in Cd-based alloy systems resulting in the discovery of stable icosahedral phases in ternary Cd–Mg–RE and binary Cd–Yb and Cd–Ca (Guo *et al* 2000, 2001, Tsai *et al* 2000, Jiang *et al* 2001).

Anti-phase boundaries (APBs) can exist in face-centred IQCs due to chemical ordering, as shown for icosahedral Al–Cu–Fe by Devaud-Rzepski *et al* (1989) and Ebalard and Spaepen (1990). Besides that, stacking faults were observed and characterized in different IQCs (Wang *et al* 1998, Caillard *et al* 2000, Heggen *et al* 2001b). Heggen (2000), Heggen *et al* (2001a, 2002) observed APBs in plastically deformed as well as in heat-treated and subsequently quenched Zn–Mg–Dy single IQC samples. In that study, the plane normals of the APBs were found to be mostly parallel to fivefold (A5) axes for heat-treated and quenched samples and pseudo-twofold (A2P) directions for deformed material. Recently, a high resolution electron microscopy (HREM) study of an APB in a fivefold plane in Zn–Mg–Dy IQC was reported by Heggen *et al* (2001b). In this study an inverse Fourier transform lattice fringe analysis was involved to confirm the characteristics of APBs in icosahedral Zn–Mg–Dy. This technique has been successfully used earlier for the analysis of dislocations in quasicrystals by Devaud-Rzepski *et al* (1990) and Yang *et al* (1998, 2000).

In this paper we calculate the atomic positions of an IQC containing an APB utilizing a cut and projection method (cf Janot 1992). The six-dimensional (6D) atomic model of the Zn–Mg–Dy IQC is derived from the model for icosahedral Zn–Mg–Ho proposed by Ishimasa and Shimizu (2000) and Ishimasa (2001). Based on this atomic model, we calculate the exit-plane wavefunctions (EPWs) and corresponding HREM images. Finally, we analyse the APB by an inverse Fourier transform lattice fringe technique.

2. Atomic model of a Zn–Mg–Dy icosahedral quasicrystal containing an APB

2.1. Atomic model of face-centred icosahedral quasicrystal Zn–Mg–Dy

To date, the determination of the structure of icosahedral Zn-based quasicrystals is still an unresolved problem. However, a number of approximate models have been presented in recent years (Yamamoto *et al* 1996, Ohno and Ishimasa 1998, Takakura *et al* 2001). Ohno and Ishimasa (1998) proposed a crude 6D atomic structure model for the $Zn_{47}Mg_{45}Ho_8$ IQC phase by fitting powder x-ray diffraction data, showing that chemical ordering is the origin of the face-centred symmetry. Investigations revealed the ideal stoichiometry of IQCs to be located around $Zn_{60}Mg_{30}RE_{10}$ for RE = Y, Gd, Tb, Dy, Ho and Er (Tsai *et al* 1997, Langsdorf *et al* 1997, Sato *et al* 1998a, Fisher *et al* 1998, Tsai 1999). Recently, Ishimasa and Shimizu (2000) presented a modified model giving a correct composition of $Zn_{60}Mg_{30}Ho_{10}$, a reasonable mass density and a reduced occurrence of unphysically short atomic distances. However, their model is far from perfection for some shortcomings, such as the following: (1) Ho should occupy the centre of the atomic surface rather than the periphery, as argued by Takakura *et al* (2001); (2) disorder still exists in some lattice sites; (3) unphysically short atomic distances have not been completely eliminated.

We adopt this model for the description of icosahedral $Zn_{60}Mg_{30}Dy_{10}$ simply by replacing Ho with Dy. The composition of the calculated structure is then close to the composition
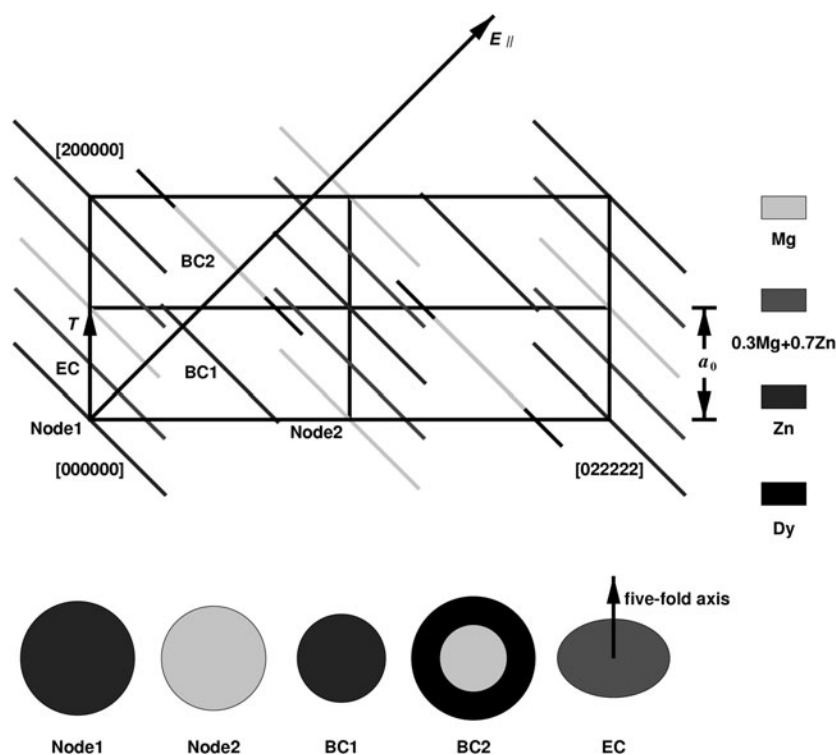
Figure 1. Hyperlattice unit cell for the structure model of face-centred Zn–Mg–Dy IQC. The cell parameters are given in table 1. T denotes the 6D translation vector, which is used as the shift vector to produce the APB.

Table 1. Hyperlattice unit-cell parameters for the structure model of the Zn–Mg–Dy IQC. The short axis of the ellipsoid at the EC node is parallel to the fivefold direction (Ishimasa 2001). The 6D lattice parameter is $a_0 = 7.3445$ Å.

	Site	Symmetry	Multiplicity	Element	Radius (Å)
Node 1	$(0, 0, 0, 0, 0, 0)$	Y_h	1	Zn	7.1
Node 2	$(1, 0, 0, 0, 0, 0)$	Y_h	1	Mg	6.5
BC1	$1/2(1, 1, 1, 1, 1, 1)$	Y_h	1	Zn	5.5
BC2	$1/2(3, 1, 1, 1, 1, 1)$	Y_h	1	Mg, Dy	4.2, 7.7
EC	$1/2(1, 0, 0, 0, 0, 0)$	C_{5v}	12	$0.3Mg + 0.7Zn$	7.0, 4.9

$Zn_{62.6}Mg_{28.3}Dy_{9.1}$ of the samples studied by Heggen *et al* (2001a, 2001b). Figure 1 schematically shows two hyperlattice unit cells and the 3D physical (parallel) space $E_\parallel$. We adopt $a_0 = 7.3445$ Å as the 6D primitive lattice parameter (Ohno and Ishimasa 1998). The 6D unit cell is face-centred hypercubic and contains five different types of atomic surface located at the nodes (node 1 and node 2) and body-centred (BC1 and BC2) and edge-centred (EC) positions of the primitive hyperlattice. The perpendicular space extensions of the atomic surfaces are listed in table 1. Note that the atomic surface on the EC position is an ellipsoid, of which the short axis is oriented parallel to the fivefold direction (Ishimasa 2001).

We used this model to calculate the atomic positions for perfect structure in a $7 \times 7 \times 7$ nm^3 box in 3D physical space. The box is confined by surfaces perpendicular to the A2P, twofold

(A2) and A5 axes. These axes were chosen to be parallel to the x, y and z axes, respectively, of the coordinate system used in the following. The number of atoms in the box amounts to 18 835, the average chemical composition is $Zn_{61.1}Mg_{29.4}Dy_{9.5}$ and the density is about 5.7 g cm^{-3}. Both the composition and density agree with experimentally determined values (Ishimasa and Shimizu 2000). Figures 2(a) and (b) show the projection of atoms in the box along A5 and A2 axes respectively. In these figures the open, grey, dark grey and full circles denote Mg, 0.3Mg + 0.7Zn, Zn and Dy atoms respectively. The radii of the plotted discs are chosen as a function of the z and y coordinates of the atom positions respectively, i.e., atoms closer to the top are plotted larger.

With the atom positions in the box, we calculated the corresponding EPW and HREM images employing the multi-slice technique and the EMS program package developed by Stadelmann (1987). Figures 2(c) and (d) show the corresponding EPW intensity patterns and figures 2(e) and (f) the simulated HREM images, using an accelerating voltage of 400 kV at approximate defocus values of $\Delta f = -60$ nm and a spherical aberration coefficient $C_s = 1.0$ mm. We can see the close correspondence between the projections of atom positions, EPW intensity patterns and simulated HREM images. Figure 2(e) shows the same characteristics as an experimental HREM image along an A5 direction (figure 6 in Fisher *et al* 1998), which indicates the reasonableness of the atomic model used here to some extent. The EPW shows the characteristics of the studied structure, irrespective of the various transmission electron microscope parameters. Hence we will use the EPW intensity patterns rather than HREM images in the following analysis.

2.2. The shift vector along the APB

In order to compare with the primitive IQC we utilize the same coordinate system for both IQCs. In this case, the 6D lattice points for the primitive IQC should be divided into two types: even nodes with the summation of their six indices equal to an even integer; and odd nodes with the summation an odd integer. For example, nodes [0, 0, 0, 0, 0, 0], [0, 2, 2, 2, 2, 2], [2, 0, 0, 0, 0, 0], [2, 2, 2, 2, 2, 2] and [1, 1, 1, 1, 1, 1] in figure 1 are even nodes, and nodes [0, 1, 1, 1, 1, 1], [1, 0, 0, 0, 0, 0], [1, 2, 2, 2, 2, 2] and [2, 1, 1, 1, 1, 1] in figure 1 are odd nodes. A unit cell of a face-centred IQC consists of two primitive unit cells, represented by one even node and its neighbour odd node. Similarly, the 6D reciprocal lattice vectors for a face-centred IQC should be divided into two types: fundamental ones with their indices all integers, which are common for both primitive and face-centred IQCs, and superlattice reciprocal vectors with their indices all half odd-integers, which are specific to face-centred IQCs.

In their experimental study on planar defects, by using diffraction contrast imaging technique, Heggen *et al* (2001a) found that the planar defects investigated are visible in diffraction contrast images if a superlattice reflection G^S is activated for diffraction contrast imaging, whereas no contrast is observed if any fundamental reflection G^F is used. This fact reveals that any lattice vector T of odd nodes, e.g., $T = [1, 0, 0, 0, 0, 0]$, may be selected as the shift vector of the APB, because $G^S \cdot T$ is equal to a half integer which corresponds to a phase change of π. This fact is the origin of the name 'anti-phase boundary' for this planar defect. From figure 1, it is obvious that the 6D translation vector $T = [1, 0, 0, 0, 0, 0]$, which is parallel to [1/0, 0/1, 0/0] in physical space, is not a symmetry operation of the face-centred IQC lattice and hence can be chosen as an APB fault vector. The APB is then introduced into the structure according to the geometry shown in figure 3(b) by giving the atoms in the right-hand side of the box a translation of $T = [1, 0, 0, 0, 0, 0]$ in 6D space.
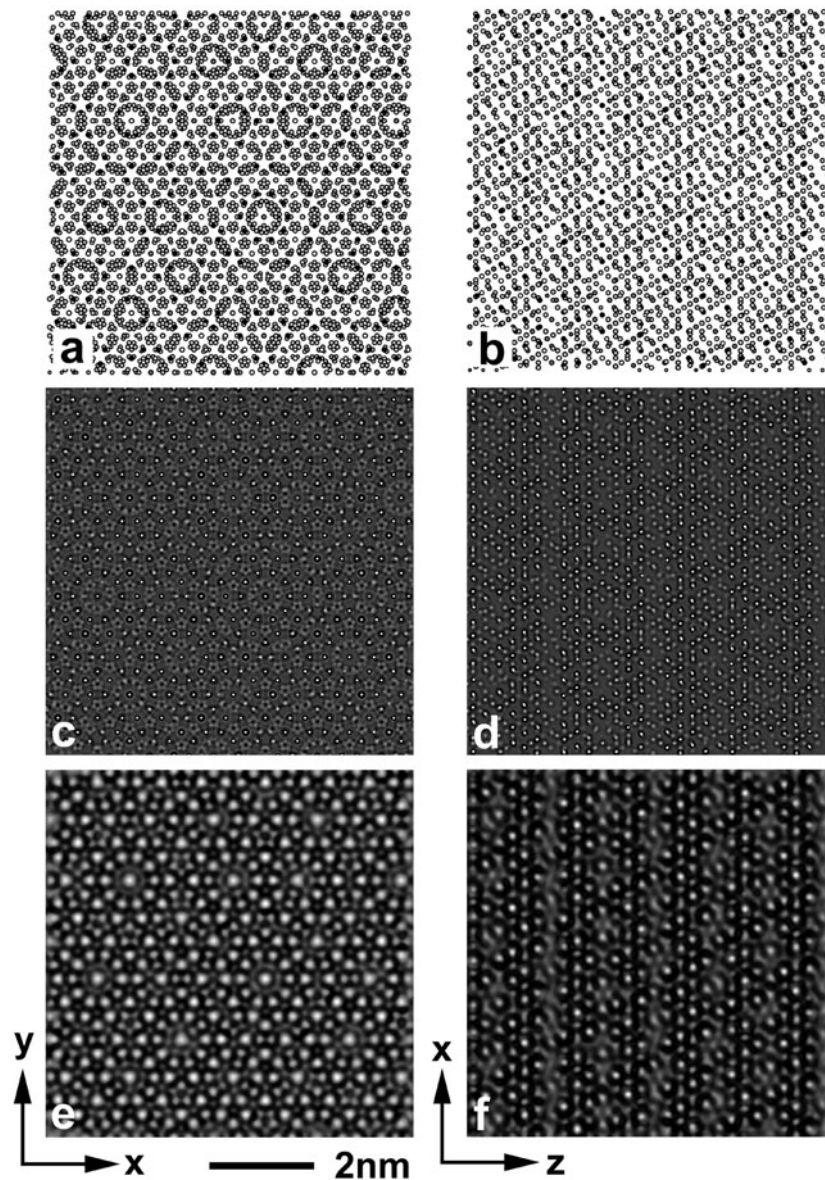
Figure 2. Perfect structure of face-centred Zn–Mg–Dy IQC according to the structure model defined in table 1 and figure 1. Physical-space atomic positions projected along (a) A5 and (b) A2 directions. The open, grey, dark grey and full circles denote Mg, $0.3Mg + 0.7Zn$, Zn and Dy atoms respectively. Corresponding EPW intensity patterns (c) and (d), and simulated HREM images (e) and (f).

2.3. Atomic model of face-centred Zn–Mg–Dy IQC containing an APB

According to the experimental findings of Heggen *et al* (2001a, 2002), the APB normal is chosen along a fivefold direction. Cahn *et al* (1986) showed that superstructure reflections due to face-centred ordering can be visible in twofold diffraction patterns. Hence we choose
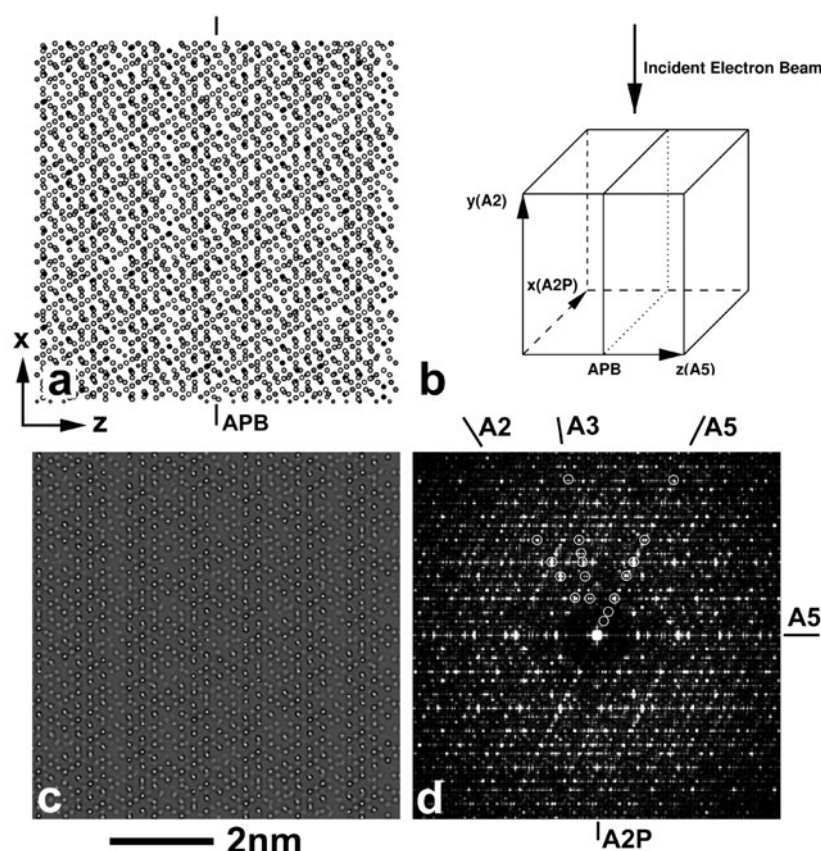
Figure 3. (a) Physical-space atomic positions projected along the y (A2) axis of the structure which contains an APB perpendicular to the z (A5) axis. (b) Geometry of the defected structure containing the APB. (c) EPW intensity pattern corresponding to (a). (d) Fourier transform of (c). The marked spots correspond to the reflections used for inverse transformation. Labelling (table 2): along A2 $g_{21}, g_{22}, \ldots, g_{24}$, along A3 $g_{31}, g_{32}, \ldots, g_{36}$ and along A5 $g_{51}, g_{52}, \ldots, g_{57}$ sequentially from the centre.

a viewing direction (i.e. the direction of incident electron beam in the HREM simulations) parallel to an A2 axis.

The atom positions in physical space (figure 3(a)) are calculated via a cut-and-projection formalism (Janot 1992) after introduction of the APB. The number of atoms in the box containing the fault amounts to 18 842, the composition is $Zn_{61.2}Mg_{29.3}Dy_{9.5}$ and the density is 5.7 g cm^{-3}. In these properties, the structure containing the APB is thus very close to the ideal structure. Minor differences occur due to the boundary effects. The corresponding EPW intensity pattern shown in figure 3(c) is calculated with the EMS program package using the same parameters as those for the perfect one (figure 2(d)).

Figure 3(d) shows the central part of the numerical Fourier transform of the EPW intensity pattern in figure 3(c). Circles mark those spots which have been used for the inverse Fourier transformations shown in figure 4. Their indices are listed in table 2.

Figure 4 shows lattice fringe images obtained by inverse Fourier transformation of figure 3(d). When superstructure reflection spots are used for back-transformation (g_{31}, g_{54}, g_{56} for figures 4(b), (d) and (f)), the APB is visible. When crossing the APB, bright lattice fringes
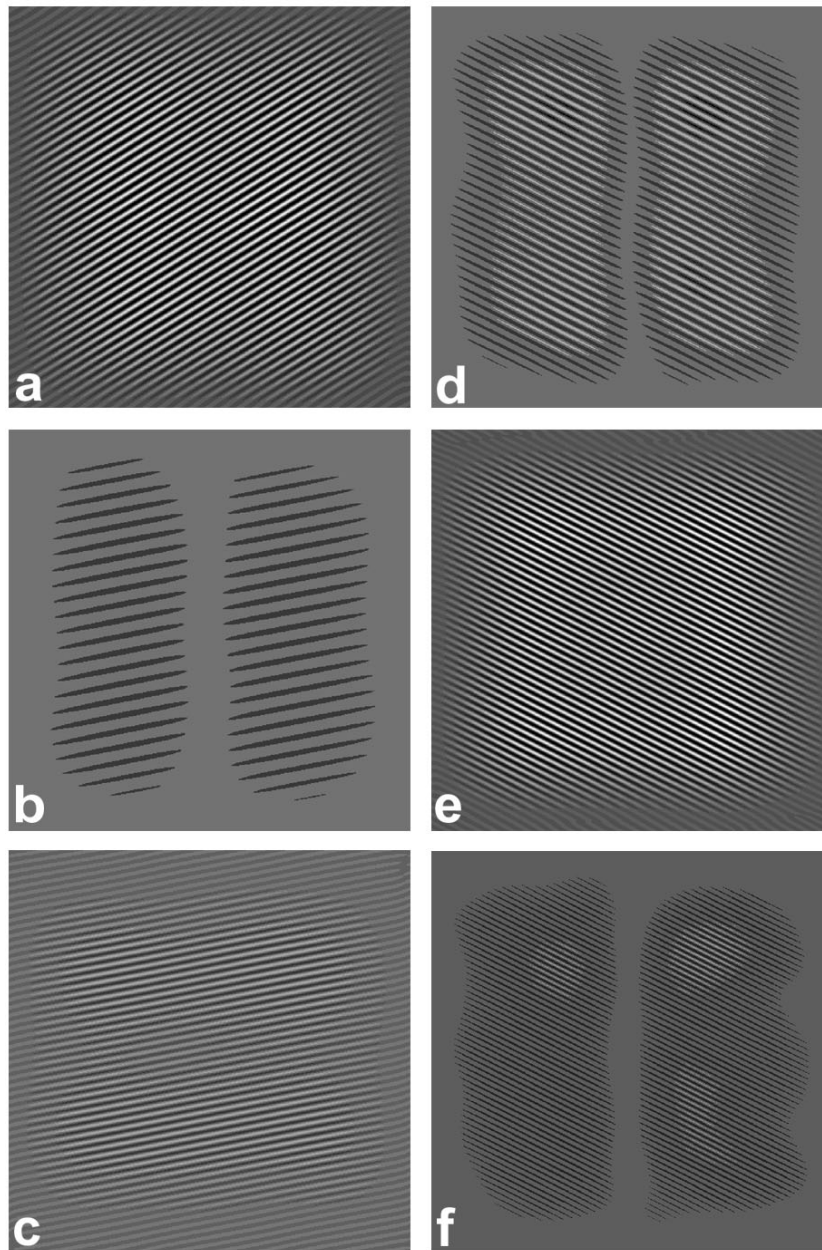
Figure 4. Fringe patterns obtained by inverse Fourier transformation using the reflections (a) g_{22}, (b) g_{31}, (c) g_{33}, (d) g_{54}, (e) g_{55} and (f) g_{56}. (See table 2.)

are found to turn into dark ones, and vice versa. When fundamental reflections are used for back-transformation (g_{22}, g_{33}, g_{55} for figures 4(a), (c) and (e)), the APB is not visible. The complete results of this analysis are listed in table 2.

We have additionally performed the simulation of an APB perpendicular to an A2P axis (x axis in figure 3(b)). This APB orientation has frequently been observed in experimental studies in deformed samples (Heggen *et al* 2000b, 2001a, 2002). For such an oriented APB,

Table 2. Results of the lattice-fringe analysis of the APB. g denotes all diffraction vectors used and their physical space $(h/h', k/k', l/l')$ and 6D indices $(n_1, n_2, n_3, n_4, n_5, n_6)$ according to Cahn *et al* (1986). F, fundamental reflection; S, superstructure reflection.

Label	$(h/h', k/k', l/l')$	$(n_1, n_2, n_3, n_4, n_5, n_6)$	Fundamental or superstructure reflection (F/S)	Shift of fringes at APB Yes or no (Y/N)
g_{21}	(2/4, 0/0, 0/0)	(1, 2, 0, −1, 2, 0)	F	N
g_{22}	(4/6, 0/0, 0/0)	(2, 3, 0, −2, 3, 0)	F	N, figure 4(a)
g_{23}	(4/8, 0/0, 0/0)	(2, 4, 0, −2, 4, 0)	F	N
g_{24}	(6/10, 0/0, 0/0)	(3, 5, 0, −3, 5, 0)	F	N
g_{31}	(2/3, 1/1, 0/0)	1/2(3, 3, 1, −1, 3, −1)	S	Y, figure 4(b)
g_{32}	(3/5, 1/2, 0/0)	1/2(5, 5, 1, −1, 5, −1)	S	Y
g_{33}	(4/6, 2/2, 0/0)	(3, 3, 1, −1, 3, −1)	F	N, figure 4(c)
g_{34}	(5/7, 2/3, 0/0)	1/2(7, 7, 3, −3, 7, −3)	S	Y
g_{35}	(5/8, 2/3, 0/0)	(4, 4, 1, −1, 4, −1)	F	N
g_{36}	(8/13, 3/5, 0/0)	1/2(13, 13, 3, −3, 13, −3)	S	Y
g_{51}	(0/1, 1/1, 0/0)	1/2(1, 1, 1, 1, 1, −1)	S	Y
g_{52}	(1/1, 1/2, 0/0)	1/2(3, 1, 1, 1, 1, −1)	S	Y
g_{53}	(1/2, 2/3, 0/0)	(2, 1, 1, 1, 1, −1)	F	N
g_{54}	(2/3, 3/5, 0/0)	1/2(7, 3, 3, 3, 3, −3)	S	Y, figure 4(d)
g_{55}	(2/4, 4/6, 0/0)	(4, 2, 2, 2, 2, −2)	F	N, figure 4(e)
g_{56}	(3/5, 5/8, 0/0)	1/2(11, 5, 5, 5, 5, −5)	S	Y, figure 4(f)
g_{57}	(5/8, 8/13, 0/0)	(9, 4, 4, 4, 4, −4)	F	N

we found similar results as listed in table 2. Namely, the APB is visible in lattice-fringe images if superlattice reflections are used for inverse Fourier transformation, while the lattice fringes are undistorted if fundamental reflections are used.

Figure 5 shows the statistics about changes of the atom distribution caused by an APB which lies at the position $z = 35$ Å and is perpendicular to the A5 axis. Circles and triangles represent respectively the atoms in the perfect and APB-defected IQCs. These statistics reveal the following.

(1) The APB does not affect the distribution of the $0.3Mg + 0.7Zn$ atoms. This fact is easily understood if we notice that the 12 EC positions are the same for both even and odd nodes in the 6D atomic model (figure 1).

(2) Zn atoms are pushed away from the APB and Mg and Dy atoms are pulled to the APB.

For example, when starting from the APB, the first two layers of Zn atoms lying at the positions of $z = 35.596$ and 36.483 Å in the perfect face-centred IQC are shifted to the positions of $z = 37.031$ and 37.918 Å in the APB-containing face-centred IQC by an amount of 1.435 Å. At the same time, the Mg atoms lying at the positions of $z = 37.031$ and 37.918 Å are pushed to the positions of $z = 35.596$ and 36.483 Å. The Dy atoms at the position of $z = 37.918$ Å are pushed to the position of $z = 35.596$ Å.

Similar statistics were carried out for the APB lying at the position of $x = 35$ Å and perpendicular to the A2P axis as shown in figure 6. Surprisingly there is only very little change of the atomic distribution for all types of atom except some shifts in the planes which are parallel to the APB plane.

These statistics tell us that the APB perpendicular to an A5 axis is non-conservative, while the APB perpendicular to an A2P axis is nearly conservative.
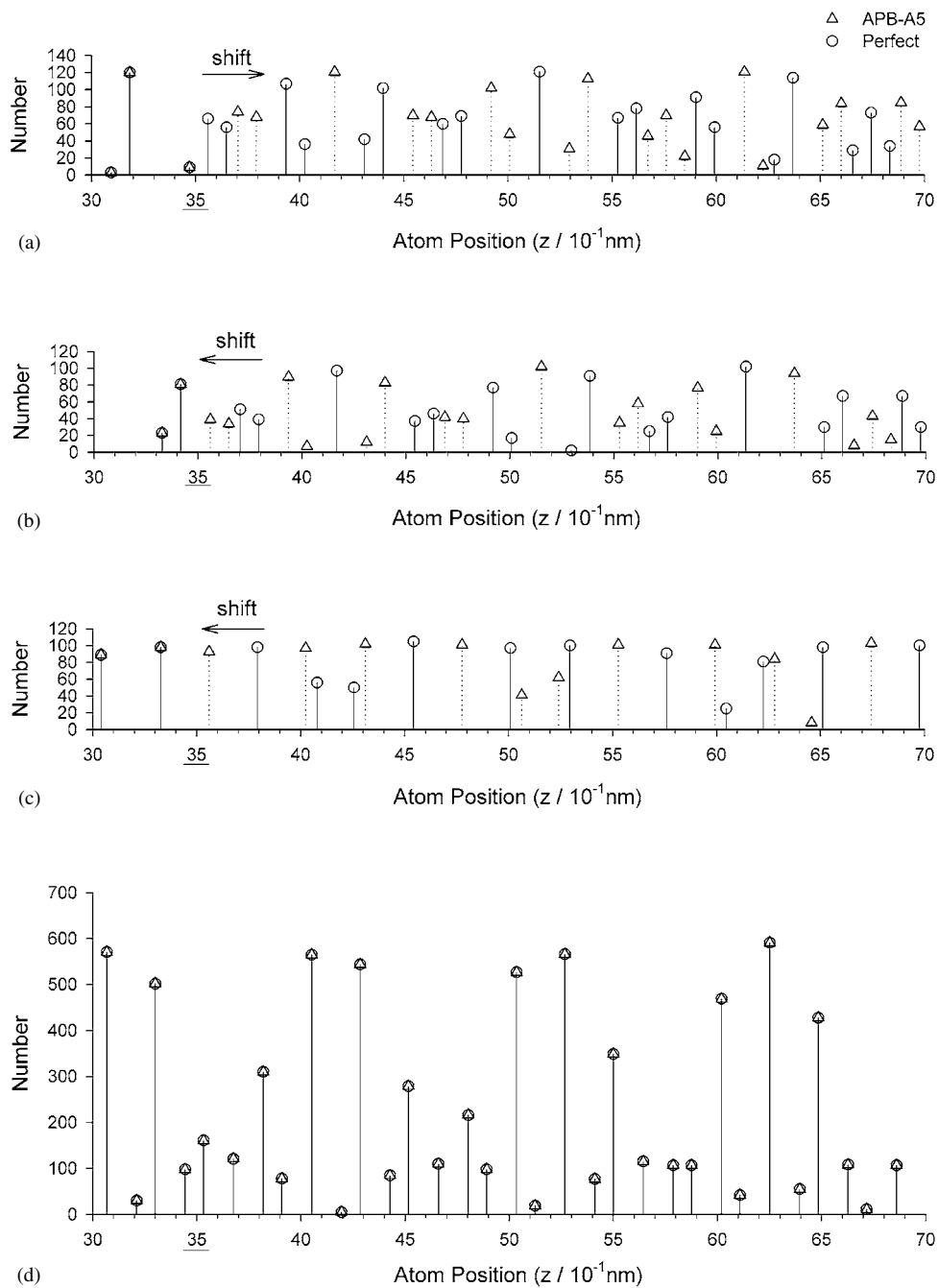
Figure 5. Statistical changes of the atom distribution caused by an APB which lies at the position $z = 35$ Å and is perpendicular to the A5 axis. Circles and triangles represent respectively the atoms in the perfect and APB-defected IQCs. (a) Zn atoms; (b) Mg atoms; (c) Dy atoms; (d) 0.3Mg + 0.7Zn atoms.
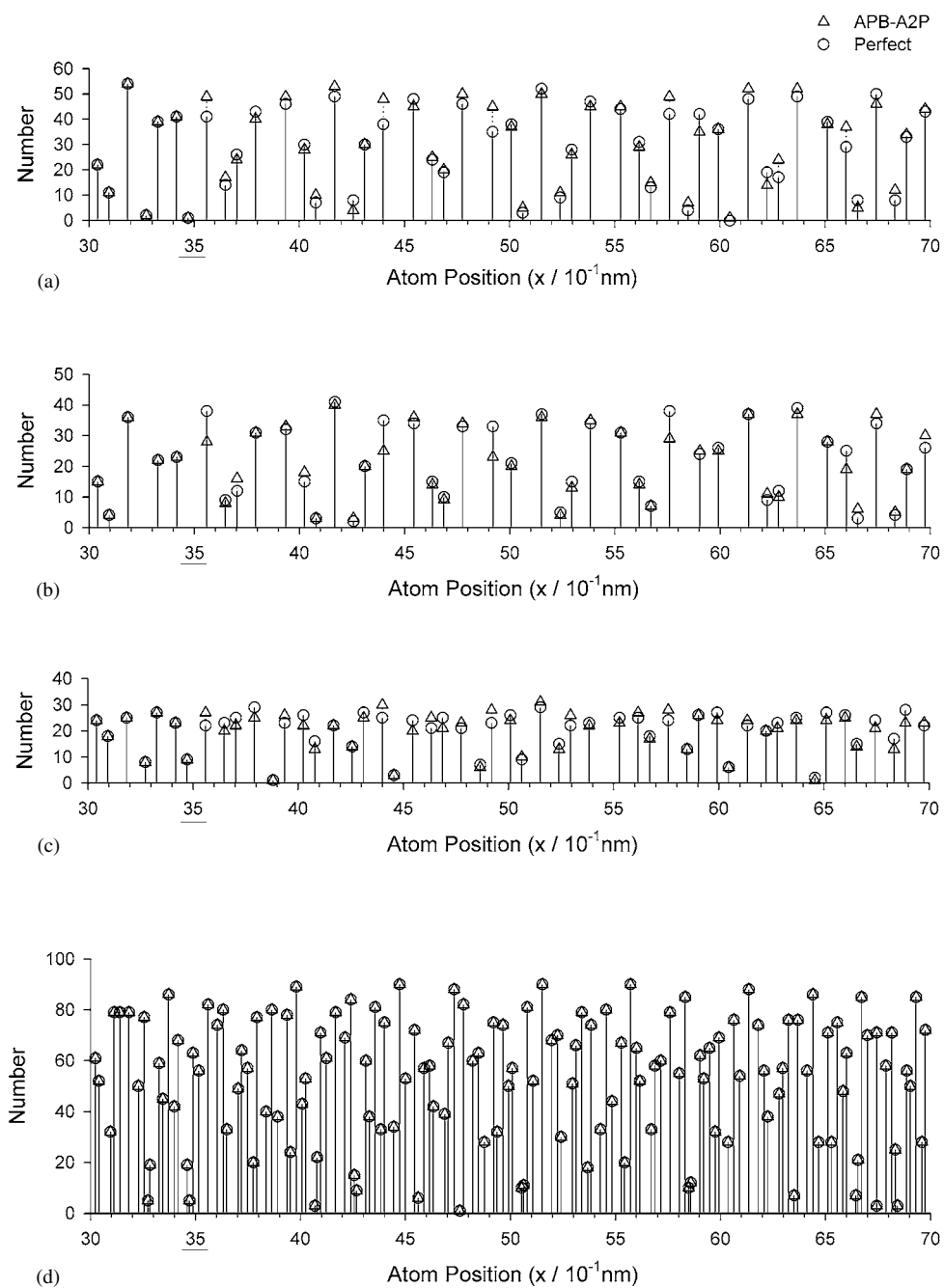
Figure 6. Statistical changes of the atom distribution caused by an APB which lies at the position $x = 35$ Å and is perpendicular to the A2P axis. Circles and triangles represent respectively the atoms in the perfect and APB-defected IQCs. (a) Zn atoms; (b) Mg atoms; (c) Dy atoms; (d) 0.3Mg + 0.7Zn atoms.

3. Discussion

In this paper we present the simulation of an APB on the basis of an atomic model of the face-centred Zn–Mg–Dy IQC. The APB was introduced by a shift vector in the 6D hyperlattice and the atomic positions of the physical-space structure containing the defect were obtained by subsequent application of a cut-and-projection formalism. Calculated EPWs of the defected structure were characterized using an inverse Fourier transform lattice-fringe technique. This allows a direct comparison with a corresponding experimental study recently published by Heggen *et al* (2001b). In that study, the authors found that the planar defects are visible in lattice-fringe images if superlattice reflections are used for inverse Fourier transformation, whereas the lattice fringes of fundamental reflections are undistorted. The same results are obtained in the present study, indicating that our approach for the construction of the APB gives useful results.

An APB with a shift vector of $T = [1, 0, 0, 0, 0, 0]$ ending in the interior of a grain has to be bounded by a partial dislocation with a Burgers vector of $B_P = [1, 0, 0, 0, 0, 0]$ which is parallel to $[1/0, 0/1, 0/0]$ in physical space. Even in face-centred cubic crystals, it is very difficult to identify the Burgers vector of a partial dislocation, because the extinction condition is not simply $g \cdot b_P = 0$ (Hirsch *et al* 1965). Moreover, a partial dislocation of a Burgers vector $B_P = [1, 0, 0, 0, 0, 0]$ may be decomposed further, forming a stacking fault in between as Heggen (2000, figure 4.17) observed. All these facts complicate the experimental examination of the partial dislocations bounding the APB in the face-centred IQC.

Heggen *et al* (2001a) observed experimentally that crossing of two APBs leads to their annihilation at their intersection line and illustrated this phenomenon schematically by a two-dimensional ordered crystal. In fact, this phenomenon can be interpreted easily by the 6D atomic model of APB utilized in the present paper. Notice that the difference between the face-centred and simple lattices lies in the fact that for a simple lattice all the vectors $[n_1, n_2, n_3, n_4, n_5, n_6]$ with integer indices n_k are lattice vectors, while for a face-centred lattice only those with even sums of the indices ($\sum n_k =$ even) are lattice vectors, and the vectors with odd sum indices are translation vectors between two anti-phase domains. By the language of group theory, this is to say that the index of the subgroup H pertaining to the face-centred lattice is 2 compared with its supergroup G pertaining to the simple lattice. The corresponding decomposition is as follows:

$$G = H + TH,$$

with

$$G = \{[n_1, n_2, n_3, n_4, n_5, n_6] | n_k \subset Z\},$$
$$H = \left\{ [n_1, n_2, n_3, n_4, n_5, n_6] | n_k \subset Z \text{ and } \sum n_k = \text{ even} \right\},$$
$$T = [1, 0, 0, 0, 0, 0],$$

where Z denotes the integer group. According to this atomic model, there are only two types of anti-phase domain with a translation vector of $T = [1, 0, 0, 0, 0, 0]$ in between. Other translation vectors are all equivalent to this. For example, $T' = [0, 1, 1, 1, 1, 1] = [1, 0, 0, 0, 0, 0] + [-1, 1, 1, 1, 1, 1]$. Hence, crossing of two APBs leads to their annihilation at their intersection line.

As shown in figures 3(d) and 4, the intensity of superstructure reflection spots and the contrast of the corresponding inverse Fourier transformed images are very weak compared with the experimental observations (Heggen *et al* 2001b). We have noted that, using the model by Ishimasa and Shimizu (2000), Ishimasa (2001), about 70% of the physical-space atomic

positions obtained are 0.3Mg + 0.7Zn from the EC sites in the 6D lattice. These, however, do not contribute to the intensity of superstructure reflection spots and therewith to the APB. This fact indicates an insufficient ordering in the model proposed by Ishimasa and Shimizu (2000), Ishimasa (2001).

A surprising conclusion obtained from the statistics about changes of the atom distribution caused by an APB reveal that the APB perpendicular to an A5 axis (APB-A5) is non-conservative, while the APB perpendicular to an A2P axis (APB-A2P) is nearly conservative. It is well known that the formation of a non-conservative APB needs diffusion. This fact is consistent with the recent experimental observation (Heggen *et al* 2002) that the frequency of occurrence of APB-A5 is 90% in the heat-treated samples compared with that in the deformed samples (45%), while the frequency of occurrence of APB-A2P is 34% in the deformed samples compared with that in the heat-treated samples.

Acknowledgments

References

Cahn J W, Shechtman D and Gratias D 1986 *J. Mater. Res.* **1** 13
Caillard D, Vanderschaeve G, Bresson L and Gratias D 2000 *Phil. Mag.* A **80** 237
Charrier B, Ouladdiaf B and Schmitt D 1997 *Phys. Rev. Lett.* **78** 4637
Devaud-Rzepski J, Cornier-Quiquandon M and Gratias D 1990 *Quasicrystals and Incommensurate Structures in Condensed Matter* ed M J Yacaman, D Romeu, V Castano and A Gomez (Singapore: World Scientific) p 498
Devaud-Rzepski J, Quivy A, Calvayrac Y, Cornier-Quiquandon M and Gratias D 1989 *Phil. Mag.* B **60** 855
Ebalard S and Spaepen F 1990 *J. Mater. Res.* **5** 62
Fisher I R, Islam Z, Panchula A F, Cheon K O, Kramer M J, Canfield P C and Goldman A I 1998 *Phil. Mag.* B **77** 1601
Guo J Q, Abe E and Tsai A P 2000 *Phys. Rev.* B **62** R14605
Guo J Q, Abe E and Tsai A P 2001 *Phil. Mag. Lett.* **81** 17
Heggen M 2000 *Diplomarbeit* RWTH-Aachen p 65
Heggen M, Feuerbacher M, Schall P, Klein H, Fisher I R, Canfield P C and Urban K 2000a *Phil. Mag. Lett.* **80** 129
Heggen M, Feuerbacher M, Schall P, Klein H, Fisher I R, Canfield P C and Urban K 2000b *Mater. Sci. Eng.* A **294–296** 781
Heggen M, Feuerbacher M, Schall P, Urban K and Wang R 2001a *Phys. Rev.* B **64** 014202
Heggen M *et al* 2001b at press
Heggen M, Feuerbacher M, Lange T and Urban K 2002 *J. Alloys Compounds* **342** 330
Hirsch P, Howie A, Nicholson R B, Pashley D W and Whelan M J 1965 *Electron Microscopy of Thin Crystals* (London: Butterworths) p 267
Ishimasa T and Shimizu T 2000 *Mater. Sci. Eng.* A **294–296** 232
Ishimasa T 2001 private communication
Janot C 1992 *Quasicrystals: a Primer* (Oxford: Clarendon) p 97
Jiang J Z, Jensen C H, Rasmussen A R and Gerward L 2001 *Appl. Phys. Lett.* **78** 1856
Langsdorf A, Ritter F and Assmus W 1997 *Phil. Mag. Lett.* **75** 381
Luo Z, Zhang S, Tang Y and Zhao D 1993 *Scr. Metall. Mater.* **28** 1513
Matsuo S, Ishimasa T and Nakano H 2000 *Mater. Sci. Eng.* A **294–296** 633
Niikura A, Tsai A P, Inoue A and Masumoto T 1994a *Phil. Mag. Lett.* **69** 351

Niikura A, Tsai A P, Inoue A and Masumoto T 1994b *Japan. J. Appl. Phys.* **33** L1538
Ohno T and Ishimasa T 1998 *Proc. 6th Int. Conf. on Quasicrystals (Tokyo)* ed S Takeuchi and T Fujiwara (Singapore: World Scientific) p 39
Sato T J, Takakura H and Tsai A P 1998a *Japan. J. Appl. Phys.* **37** L663
Sato T J, Takakura H, Tsai A P and Shibata K 1998b *Phys. Rev. Lett.* **81** 2364
Stadelmann P A 1987 *Ultramicroscopy* **21** 131
Takakura H, Shiono M, Sato T J, Yamamoto A and Tsai A P 2001 *Phys. Rev. Lett.* **86** 236
Tsai A P 1999 *Physical Properties of Quasicrystals* ed Z M Stadnik (Berlin: Springer) p 5
Tsai A P, Guo J Q, Abe E, Takarura H and Sato T J 2000 *Nature* **408** 537
Tsai A P, Niikura A, Inoue A and Masumoto T 1997 *J. Mater. Res.* **12** 1997
Tsai A P, Niikura A, Inoue A, Masumoto T, Nishida Y, Tsuda K and Tanaka M 1994 *Phil. Mag. Lett.* **70** 169
Wang R, Feuerbacher M, Yang W and Urban K 1998 *Phil. Mag.* A **78** 273
Yamamoto A, Weber S, Sato A, Kato K, Ohshima K, Tsai A P, Niikura A, Hiraga K, Inoue A and Masumoto T 1996 *Phil. Mag. Lett.* **73** 247
Yang W, Feuerbacher M, Tamura N, Ding D H, Wang R and Urban K 1998 *Phil. Mag.* A **77** 1481
Yang W, Wang R, Feuerbacher M, Schall P and Urban K 2000 *Phil. Mag. Lett.* **80** 281